Author(s): Kostensalo, Joel; Suhonen, Jouni

Title: Mesonic enhancement of the weak axial charge and its effect on the half-lives and spectral shapes of first-forbidden J+↔J− decays

Year: 2018

Version:

Please cite the original version:

Kostensalo, J., & Suhonen, J. (2018). Mesonic enhancement of the weak axial charge and its effect on the half-lives and spectral shapes of first-forbidden J+↔J− decays. Physics Letters B, 781, 480-484. https://doi.org/10.1016/j.physletb.2018.02.053

Physics Letters B 781 (2018) 480–484

Contents lists available at ScienceDirect

Physics Letters B

www.elsevier.com/locate/physletb

Mesonic enhancement of the weak axial charge and its effect on the half-lives and spectral shapes of first-forbidden $J^+ \leftrightarrow J^-$ decays

Joel Kostensalo *, Jouni Suhonen

University of Jyvaskyla, Department of Physics, P. O. Box 35, FI-40014, Finland

ARTICLE INFO

Article history:
Received 8 November 2017
Accepted 21 February 2018
Available online 26 February 2018
Editor: W. Haxton

Keywords:
Meson-exchange currents
Weak interactions
Nuclear medium effects
Forbidden beta decays
Spectral shape

ABSTRACT

The effects of the enhancement of the axial-charge matrix element γ_5 were studied in medium heavy and heavy nuclei for first-forbidden $J^+ \leftrightarrow J^-$ decay transitions using the nuclear shell model. Noticeable dependence on the enhancement $\epsilon_{\rm MEC}$ of the axial-charge matrix element, as well as on the value of the axial-vector coupling constant $g_{\rm A}$ was found in the spectral shapes of ^{93}Y, ^{95}Sr, and ^{97}Y. The importance of the spectrum of ^{138}Cs in the determination of $g_{\rm A}$ is discussed. Half-life analyses in the $A \approx 95$ and $A \approx 135$ regions were done, and consistent results $g_{\rm A} \approx 0.90$, 0.75, and 0.65, corresponding to the three enhancement scenarios $\epsilon_{\rm MEC} = 1.4$, 1.7, and 2.0, were obtained. Connection to the reactor-antineutrino anomaly is pointed out.

The enhancement of the axial-charge nuclear matrix element (NME) γ_5 due to nuclear medium effects in the form of meson-exchange currents was first suggested nearly four decades ago [1–3]. An enhancement of 40–70% over the impulse-approximation value was predicted based on chiral-symmetry arguments and soft-pion theorems. This enhancement is fundamental in nature and insensitive to nuclear-structure aspects [4,5]. Systematic shell-model studies of the γ_5 matrix elements in the $A \approx 16$, $A \approx 40$, and $A \approx 208$ regions indicated enhancements of 60–100% [6–8]. In [9] the exceptionally large enhancement of the γ_5 NME in heavy nuclei, witnessed in the shell-model studies of Warburton [8], was reproduced by introducing an effective Lagrangian incorporating approximate chiral and scale invariance of the QCD.

The non-trivial dependence of the spectral shapes of the fourth-forbidden non-unique decays of ^{113}Cd and ^{115}In on the effective value of the axial-vector coupling constant $g_{\rm A}$ was first pointed out in Ref. [10]. A new method, coined the spectrum-shape method (SSM), where theoretical and experimental spectra are compared was proposed as a complementary way to the half-life comparison method for extraction of the effective value of $g_{\rm A}$. Further investigations in [11] and [12] found that several other non-unique decays exhibit a similar dependence. It was also pointed out in [11–13] that the spectral shapes of many studied decays are practically indifferent to the fine details of the wave functions, making the spectrum-shape method a potentially much more robust tool than the often used half-life method.

Since the γ_5 NME is one of the two rank-zero matrix elements contributing to first-forbidden $\Delta J = 0$ transitions it plays quite an important role in the decay rates of many of these transitions. Therefore, a significant enhancement of this matrix element can also affect the shapes of the corresponding beta spectra. In the present Letter we investigate the impact of the γ_5 enhancement on half-lives and shapes of beta spectra for several first-forbidden $J^+ \leftrightarrow J^-$ decay transitions in the $A \approx 95$, $A \approx 135$, and $A \approx 208$ regions. Decays with beta spectra which have a significant dependence on the enhancement of the axial-charge matrix element could potentially be used to extract the enhancement in a similar way to the extraction of the effective value of $g_{\rm A}$. The importance of the consideration of the meson-exchange-current effects on beta spectra used in the reactor-antineutrino analyses and for characterization of the background radiation in rare-event searches is also pointed out.

The half-life of a forbidden non-unique beta decay can be written as

$$t_{1/2} = \kappa / \tilde{C}, \tag{1}$$

where $\kappa = 6147$ s [14] and $\tilde{C}$ is the dimensionless integrated shape function, given by

* Corresponding author.
E-mail address: joel.j.kostensalo@student.jyu.fi (J. Kostensalo).

https://doi.org/10.1016/j.physletb.2018.02.053

$$\tilde{C} = \int_1^{w_0} C(w_e) p w_e (w_0 - w_e)^2 F_0(Z, w_e) dw_e. \quad (2)$$

The shape factor $C(w_e)$ of Eq. (2) contains complicated combinations of both (universal) kinematic factors and nuclear form factors. The nuclear form factors can be related to the corresponding NMEs using the impulse approximation. For the first-forbidden non-unique decays with $J_i = J_f$, considered in this work, the relevant NMEs are those of the transition operators denoted here by $\mathcal{O}(0^-)$, $\mathcal{O}(1^-)$, and $\mathcal{O}(2^-)$. We adopt the expansion of Behrens and Bühring [15], where in the leading order in the non-relativistic reduction there are six matrix elements corresponding to the operators

$$\mathcal{O}(0^-) : g_A(\boldsymbol{\sigma} \cdot \mathbf{p}_e), \quad g_A(\boldsymbol{\sigma} \cdot \mathbf{r}) \quad (3)$$

$$\mathcal{O}(1^-) : g_V \mathbf{p}_e, \quad g_A(\boldsymbol{\sigma} \times \mathbf{r}), \quad g_V \mathbf{r} \quad (4)$$

$$\mathcal{O}(2^-) : g_A[\boldsymbol{\sigma} \mathbf{r}]_2, \quad (5)$$

where $\mathbf{r}$ is the radial coordinate and $\mathbf{p}_e$ is the electron momentum. In this work the enhancement factor of the γ_5 NME ($\boldsymbol{\sigma} \cdot \mathbf{p}_e$ in the non-relativistic limit) is denoted by ϵ_{MEC}. In addition to these six NMEs, there are three NMEs corresponding to the operators $g_A(\boldsymbol{\sigma} \cdot \mathbf{r})$, $g_A(\boldsymbol{\sigma} \times \mathbf{r})$, and $g_V \mathbf{r}$ with the Coulomb factor $\mathcal{I}(1,1,1,1;r)$ included in the radial integral. The Coulomb factor is given by [15]

$$\frac{2}{3}\mathcal{I}(1,1,1,1;r) = \begin{cases} 1 - \frac{1}{5}\frac{r}{R}, & 0 < r < R \\ \frac{R}{r} - \frac{1}{5}\left(\frac{R}{r}\right)^3, & r > R, \end{cases} \quad (6)$$

where R is the nuclear radius. In this work we include also the next-to-leading-order terms in the Behrens–Bühring expansion [15], which increases the number of NMEs involved in transitions up to 21. The NMEs involved in the transitions can be evaluated using the relation

$$^{V/A}\mathcal{M}^{(N)}_{KLS}(k_e, m, n, \rho) = \frac{\sqrt{4\pi}}{\hat{J}_i} \sum_{pn} {}^{V/A}m^{(N)}_{KLS}(pn)(k_e, m, n, \rho)(\Psi_f || [c^\dagger_p \tilde{c}_n]_K || \Psi_i), \quad (7)$$

where $^{V/A}m^{(N)}_{KLS}(pn)(k_e, m, n, \rho)$ is the single-particle matrix element, and $(\Psi_f || [c^\dagger_p \tilde{c}_n]_K || \Psi_i)$ is the one-body transition density (OBTD), which contains the nuclear-structure information. The atomic screening effects and radiative corrections are also included in the shape factor. The details of the scope of the formalism can be found from Ref. [13].

In the present work the electron spectra of 16 first-forbidden $\Delta J = 0$ β^- transitions were calculated using the NMEs produced by the use of the nuclear shell model. The spectra were calculated using nine different scenarios including all combinations of $\epsilon_{\text{MEC}} = 1.40$, 1.70, 2.00 corresponding to 40%, 70% and 100% enhancements of the axial-charge matrix element and $g_A = 0.6$, 1.00, and 1.27 corresponding to the heavily quenched, quenched, and free-nucleon values of the axial-vector coupling constant. The nuclear-structure calculations were done using the shell-model code NuShellX@MSU [16], with appropriate model spaces and Hamiltonians chosen for the three mass regions separately.

For the decay transitions in the mass range $A = 92$–97 a model space including the proton orbitals $0f_{5/2}$, $1p_{3/2}$, $1p_{1/2}$, and $0g_{9/2}$ and the neutron orbitals $1d_{5/2}$, $1d_{3/2}$, and $0s_{1/2}$ were used together with the interaction glbepn [17]. The interaction glbepn is a bare G-matrix interaction which has an adjusted version glepn, where two-body matrix elements from Gloeckner [18] and Ji and Wildenthal [19] have been adopted. The half-lives calculated using the interactions glbepn and glepn agreed for ^{96}Y to 2%, but for example for ^{93}Y the modified interaction was unable to reproduce the experimental half-life with any physically meaningful value of g_A and ϵ_{MEC}. The bare G-matrix interaction, on the other hand, was able to reproduce the experimental half-lives, ranging from less than a second to several days. Therefore the half-life analysis was done using this interaction. The decay transitions in the mass range $A = 133$–139 were calculated using a model space spanned by the proton orbitals $0g_{7/2}$, $1d_{5/2}$, $1d_{3/2}$, $2s_{1/2}$, and $0h_{11/2}$ and the neutron orbitals $0h_{9/2}$, $1f_{7/2}$, $1f_{5/2}$, $2p_{3/2}$, $2p_{1/2}$, and $0i_{13/2}$ with the effective interactions jj56pnb [20] and jj56cdb [21]. For the decays of ^{142}Pr and ^{143}Pr the dimensions of the problem were so large that truncations became necessary, and no nucleons were allowed on the $\pi 0h_{11/2}$ and $\nu 0i_{13/2}$ orbitals. This decay was not included in the half-life analysis since rather severe truncations were used. For the $A = 211$–213 nuclei the model space consisted of the proton orbitals $0h_{9/2}$, $1f_{7/2}$, $1f_{5/2}$, $2p_{3/2}$, $2p_{1/2}$, and $0i_{13/2}$ and the neutron orbitals $0i_{11/2}$, $1g_{9/2}$, $1g_{7/2}$, $2d_{5/2}$, $2d_{3/2}$, $3s_{1/2}$, and $0j_{15/2}$ with the corresponding Hamiltonian khpe [22]. Half-lives of the decays in the $A \approx 95$ and $A \approx 135$ regions were also calculated and compared with the experimental data. The effects of the mesonic enhancement on the half-lives of the first-forbidden decays in the ^{208}Pb region have been studied in detail in Ref. [8] and thus we refer to these results for the half-life part. However, the beta spectra of these decays have not been previously published.

Table 1
Decays considered in this study. The references used for the half-lives and branching ratios are given in the fourth column.

Transition	$t_{1/2}$	BR(%)	Ref.
$^{92}\text{Rb}(0^-_{g.s.}) \to {}^{92}\text{Sr}(0^+_{g.s.})$	4.492(20) s	95.2(7)	[23]
$^{93}\text{Y}(1/2^-_{g.s.}) \to {}^{93}\text{Zr}(1/2^+_1)$	10.18(8) h	2.7(5)	[24]
$^{95}\text{Sr}(1/2^+_{g.s.}) \to {}^{95}\text{Y}(1/2^-_{g.s.})$	23.90(14) s	55.7(25)	[25]
$^{96}\text{Y}(0^-_{g.s.}) \to {}^{96}\text{Zr}(0^+_{g.s.})$	5.34(5) s	95.5(5)	[26]
$^{97}\text{Y}(1/2^+_{g.s.}) \to {}^{97}\text{Zr}(1/2^-_{g.s.})$	3.75(3) s	40(10)	[27]
$^{133}\text{Sn}(7/2^-_{g.s.}) \to {}^{133}\text{Sb}(7/2^+_{g.s.})$	1.46(3) s	85(3)	[28]
$^{134}\text{Sb}(0^-_{g.s.}) \to {}^{134}\text{Te}(0^+_{g.s.})$	0.78(6) s	97.6(5)	[29]
$^{135}\text{Te}(7/2^-_{g.s.}) \to {}^{135}\text{I}(7/2^+_{g.s.})$	19.0(2) s	62(3)	[30]
$^{137}\text{Xe}(7/2^-_{g.s.}) \to {}^{137}\text{Cs}(7/2^+_{g.s.})$	3.818(13) min	67(3)	[31]
$^{138}\text{Cs}(3^-_{g.s.}) \to {}^{138}\text{Ba}(3^+_1)$	32.5(2) min	44.0(10)	[32]
$^{139}\text{Ba}(7/2^-_{g.s.}) \to {}^{139}\text{La}(7/2^+_{g.s.})$	83.06(28) min	70.0(3)	[33]
$^{139}\text{Cs}(7/2^+_{g.s.}) \to {}^{139}\text{Ba}(7/2^-_{g.s.})$	9.27(5) min	85(3)	[33]
$^{142}\text{Pr}(2^-_{g.s.}) \to {}^{142}\text{Nb}(2^+_1)$	19.12(4) h	3.7(5)	[34]
$^{143}\text{Pr}(7/2^+_{g.s.}) \to {}^{143}\text{Nb}(7/2^-_{g.s.})$	13.57(2) d	100	[35]
$^{211}\text{Pb}(9/2^+) \to {}^{211}\text{Bi}(9/2^-)$	36.1(2) min	91.32(12)	[36]
$^{213}\text{Bi}(9/2^-) \to {}^{213}\text{Po}(9/2^+)$	45.61(6) min	65.9(4)	[37]

The transitions studied in this work, the corresponding branching ratios, and the half-lives of the mother nuclei are listed in Table 1. In Table 2 are given the values of g_A needed to reproduce the experimental half-life with $\epsilon_{\text{MEC}} = 1.4$, 1.7, and 2.0 for decay transitions in the mass range $A = 91$–97. The uncertainties in the obtained g_A values stem from the uncertainty in the branching ratio and the half-life, and is given by the standard deviation $\sigma/\sqrt{N}$. The uncertainty coming from the nuclear-structure calculations is at least of the same order as the largest half-life errors, so the total uncertainty is of the order of 30% uniformly for all the decays.

The results for decays in the $A \approx 95$ region are listed in Table 2. When an enhancement of 40% for the axial-charge matrix element is assumed, an effective value close to unity is obtained

Table 2
Effective values of the coupling constant g_A for different scenarios of the enhancement of the time-like axial-vector matrix element $\int \gamma_5$ for decay transitions in the mass range $A = 92$–97. The mother nuclei are listed in the first column and the values of g_A which reproduce the experimental half-life are given in columns 2–4 for each value of ϵ_{MEC} separately. The CVC value $g_V = 1.00$ was adopted in the analysis. The error in g_A comes from the uncertainty in the branching ratio and the half-life, given by the standard deviation $\sigma/\sqrt{N}$.

Nucleus	g_A with glbepn interaction		
	$\epsilon_{mec} = 1.4$	1.7	2.0
^{92}Rb	0.74(1)	0.62(1)	0.53(1)
^{93}Y	1.25(15)	1.03(17)	0.85(30)
^{95}Sr	0.88(4)	0.70(4)	0.58(3)
^{96}Y	0.96(1)	0.80(1)	0.69(1)
^{97}Y	0.85(15)	0.70(13)	0.59(12)
Average	0.94 ± 0.08	0.77 ± 0.07	0.65 ± 0.06

for the axial-vector coupling constant g_A. For larger ϵ_{MEC} a more quenched value of g_A is required to reproduce the experimental half-lives. A previous direct calculation by Kirchbach and Reinhardt [38] for the enhancement factor resulted in $\epsilon_{MEC} = 45\%$. This would correspond to $g_A \approx 0.90$. The g_A values obtained for the 40% enhancement of the γ_5 matrix element are in line with previous shell-model results for Gamow–Teller decays in light and medium-heavy nuclei [39–41]. This is also in line with the result $g_A = 0.92$ for the fourth-forbidden decay of ^{113}Cd obtained using the spectrum-shape method with three different nuclear models [13].

For the $A \approx 135$ region the results for the effective values of g_A can be found from Table 3. The general trend is similar as for the $A \approx 95$ nuclei for both interactions: For larger enhancements of the axial-charge matrix element smaller values of g_A are needed to reproduce the experimental half-lives. The more recent jj56pnb interaction gives $g_A = 0.87 \pm 0.04$ when $\epsilon_{MEC} = 1.4$ is assumed. The result obtained using the interaction jj56cdb is in agreement with this result within error limits. For enhancement of 70% the jj56pnb agrees excellently with the result for $A \approx 95$ nuclei with $g_A = 0.75 \pm 3$. The jj56cdb result, on the other hand, is noticeably higher with $g_A = 0.87 \pm 0.06$. For $\epsilon_{MEC} = 2.0$ the shell-model results 0.70 ± 0.06 and 0.66 ± 0.03 for the $A \approx 135$ region are in harmony. This is in an astonishingly good agreement with the $A \approx 95$ result $g_A = 0.65 \pm 0.06$. This suggests that the proper effective value of g_A is the same for both the $A \approx 95$ and $A \approx 135$ regions. Our calculations suggest that an effective value of g_A below unity should be used also for first-forbidden non-unique decays with $\Delta J = 0$.

Instead of studying the effective value of g_A as a function of ϵ_{MEC}, we can of course turn this the other way around. Previous systematic studies in the $A \approx 16$ [6] and $A \approx 208$ [8] regions have resulted in enhancement factors 1.61 ± 0.03 and 2.01 ± 0.05 respectively. In addition, separate studies for ^{50}K [6] and ^{96}Y [17] yielded the enhancement factors 1.52 and 1.75 ± 0.30. Calculating

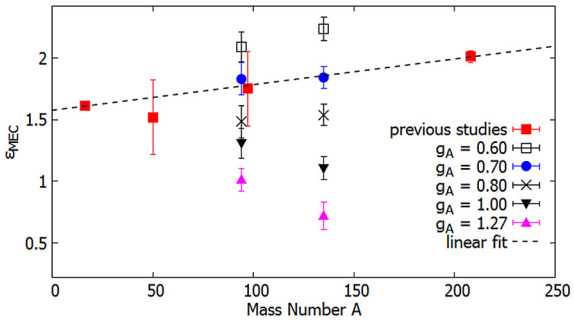

Fig. 1. The obtained enhancements ϵ_{MEC} of the previous studies and the present study as a function of the mass number A. The red squares represent the previous systematic studies done in the $A \approx 16$ and $A \approx 208$ regions and the separate studies done for ^{50}K and ^{96}Y. The other points represent the results of this study for different effective values of g_A. The linear fit is an error weighted fit, where the results of the previous studies and the previous study with $g_A = 0.70$ are used. (For interpretation of the colors in the figure(s), the reader is referred to the web version of this article.)

ϵ_{MEC} for different set values of g_A in the $A \approx 95$ and $A \approx 135$ regions and comparing to the previous results allows us to see how the mesonic enhancement behaves as a function of mass number in different scenarios. The results are presented in Fig. 1. For ^{50}K the error is assumed to be 0.30 as it is for ^{96}Y. When the free nucleon value 1.27 is adopted, no mesonic enhancement is obtained for $A \approx 95$ and for $A \approx 135$ quenching of the axial-charge matrix element is needed to reproduce the experimental half-lives. For the unity value of the axial-vector coupling constant the results are rather similar: an enhancement of only 0–20%. When $g_A = 0.70$ is adopted, a clear linear trend is seen. A fit to the data gives the relation

$$\epsilon_{MEC} = 1.576 + 2.08 \times 10^{-3}\, A. \tag{8}$$

For an even heavily quenched value, $g_A = 0.60$, an enhancement factor well above 2.0 is required to reproduce the experimental half-lives, which is not in line with the previous results. The scenario with $g_A = 0.80$, on the other hand, would result in enhancements 1.48 ± 0.13 and 1.54 ± 0.09 for the 95 and 135 regions respectively. Based on previous results this kind of scenario is also possible. The general trend in this case would not be linearly increasing, but roughly constant in the medium-heavy region.

In addition to the half-lives the shapes of the electron spectra and their dependence on g_A and ϵ_{MEC} were studied. The most interesting spectra are shown in Figs. 2–5. The spectrum related to the decay of ^{93}Y to the first $1/2^+$ state in ^{93}Zr is presented in Fig. 2. Not only is there a clear dependence on the effective value of the axial-vector coupling constant g_A, there is also a noticeable dependence on the value of ϵ_{MEC}. The spectra calculated for each scenario of the effective value of g_A are clearly distinct for any chosen ϵ_{MEC}. However, for example the combinations

Table 3
Same as Table 2 for decay transitions in the mass range $A = 133$–139 calculated using the Hamiltonians based on the jj56cdb and jj56pnb two-body interactions.

Nucleus	$g_A(\gamma_5)$ with jj56cdb int.			g_A with jj56pnb int.		
	ϵ_{mec}= 1.4	1.7	2.0	1.4	1.7	2.0
^{133}Sn	0.94(2)	0.80(2)	0.69(2)	0.94(2)	0.80(2)	0.69(2)
^{134}Sb	1.18(6)	0.99(5)	0.85(5)	0.85(4)	0.71(4)	0.62(3)
^{135}Te	0.86(2)	0.74(3)	0.65(2)	0.96(3)	0.84(3)	0.74(3)
^{137}Xe	0.74(2)	0.65(2)	0.58(2)	0.81(3)	0.71(2)	0.64(3)
^{139}Ba	0.68(1)	0.60(1)	0.54(1)	0.72(1)	0.64(1)	0.58(1)
^{139}Cs	1.15(3)	1.00(2)	0.88(2)	0.91(2)	0.79(2)	0.69(2)
Average	0.93 ± 0.08	0.87 ± 0.06	0.70 ± 0.06	0.87 ± 0.04	0.75 ± 0.03	0.66 ± 0.03

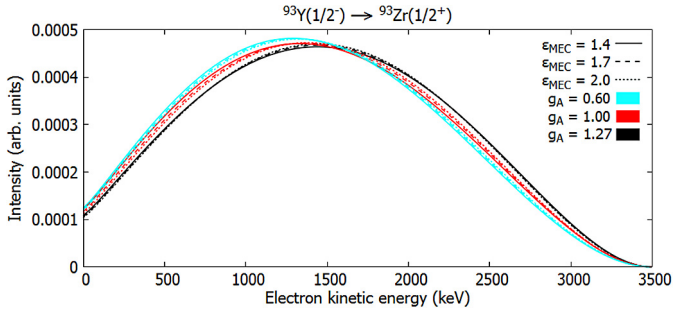

Fig. 2. Electron spectra of ^{93}Y calculated with the interaction glbepn. The color coding signifies the value of g_A and the dash coding the value of the mesonic enhancement ϵ_{MEC}.

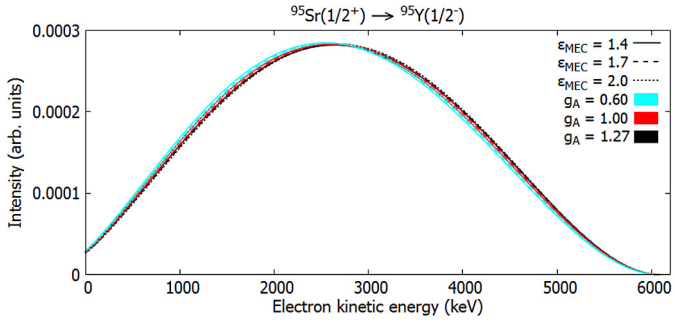

Fig. 3. Same as Fig. 2 for the decay of ^{95}Sr.

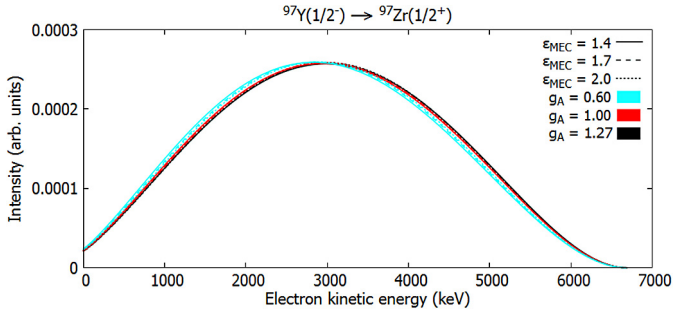

Fig. 4. Same as Fig. 2 for the decay of ^{97}Y.

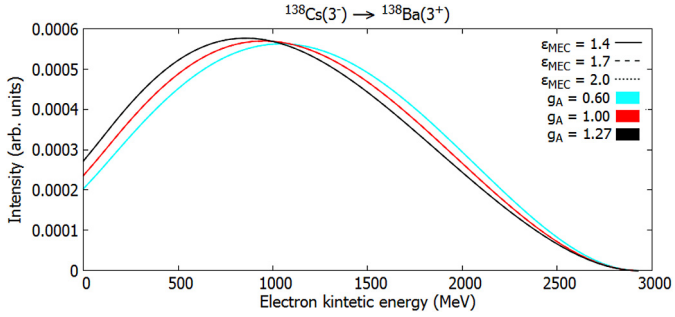

Fig. 5. Same as Fig. 2 for the decay of ^{138}Cs calculated with the jj56pnb interaction.

$(g_A, \epsilon_{MEC}) = (1.0, 1.4)$ and $(g_A, \epsilon_{MEC}) = (0.6, 2.0)$ produce spectra which are significantly closer. This is also consistent with the half-life results, where both combinations $(g_A, \epsilon_{MEC}) \approx (0.95, 1.4)$ and $(g_A, \epsilon_{MEC}) \approx (0.65, 2.0)$ reproduced the experimental half-lives. The branching ratio of this transition is 2.7 ± 5 (see Table 1), so in principal this spectrum could be measured experimentally. A high-precision measurement of this spectrum would be desirable, since it could be used to confirm the need to use quenched g_A values below unity for forbidden ΔJ transitions.

Noticeable dependence on the used g_A and ϵ_{MEC} combinations can also be seen in the spectra of ^{95}Sr and ^{97}Y presented in Figs. 3 and 4. Though the dependence is smaller than in ^{93}Y, it is very important due to the contribution of the ^{95}Sr spectrum to the cumulative beta spectrum used in reactor-antineutrino analyses [42]. Another important contributor is ^{135}Te. The dependence of the spectral shape of ^{135}Te is roughly half of that of ^{95}Sr, and is not presented here. However, these small effects are crucial when considering the significance of the reactor-antineutrino anomaly.

In addition to the decays considered in the half-life analysis, five more transitions were studied. The decay of ^{138}Cs was excluded from the half-life analysis, since the dependence of the half-life on the value of ϵ_{MEC} was practically non-existent, and thus a meaningful extraction of g_A with different values of ϵ_{MEC} was impossible. Naturally, the spectral shape of ^{138}Cs is also independent on the enhancement factor. The electron spectrum of ^{138}Cs calculated using different values of g_A is shown in Fig. 5. For this transition the dependence is significant enough that the extraction of the effective value of g_A using the spectrum-shape method is feasible to at least an accuracy of 0.1–0.2. This would be enough to see whether the value of g_A is close to unity (implying $\epsilon_{MEC} \approx 1.4$), close to 0.6 (implying $\epsilon_{MEC} \approx 2.0$), or something between. The branching ratio for this decay is 44.0 ± 10 and the Q-value is close to 3 MeV which makes an accurate measurement of the spectrum shape possible, since the experimentally problematic low-energy part of the beta spectrum is a relatively small portion in comparison with beta decays which have a Q-value of a few hundred keV.

The decays of ^{142}Pr and ^{143}Pr were also calculated to see if any significant dependence on either g_A and ϵ_{MEC} is present. For these decays, as well as for the decays of ^{211}Pb and ^{213}Bi, the dependencies turned out to be smaller than for example the dependence for ^{95}Sr and ^{97}Y. Due to the rather severe truncations used for the Pr isotopes these decays were not included in the half-life analyses.

In this Letter the significant impact of the enhancement of the axial-charge matrix element on the half-lives and spectral shapes of first-forbidden $J^+ \leftrightarrow J^-$ decay transitions was pointed out. Half-life analyses were carried out in the $A \approx 95$ and $A \approx 135$ mass regions, extracting effective values of g_A corresponding to different scenarios of the enhancement of the axial-charge matrix element, characterized by the enhancement factor ϵ_{MEC}. In both regions the effective values $g_A \approx 0.90$, 0.75, and 0.65 corresponded to the enhancement scenarios $\epsilon_{MEC} = 1.4$, 1.7, and 2.0. On the flip side, a linear dependence of ϵ_{MEC} on the mass number was found when $g_A = 0.70$ was adopted. The dependence of the beta-spectrum shape of the transition $^{93}\mathrm{Y}(1/2^-_{\mathrm{g.s.}}) \rightarrow {}^{93}\mathrm{Zr}(1/2^+_1)$ on both g_A and ϵ_{MEC} was pointed out. Similar but less significant dependencies were also recorded in the decays of ^{95}Sr and ^{97}Y. The spectrum related to the β^- decay of ^{138}Cs was found to be significantly g_A dependent, while simultaneously being independent of ϵ_{MEC}. This opens up the possibility for the determination of a proper effective value of g_A in the $A \approx 135$ region for first-forbidden decays using the spectrum-shape method. This value of g_A would also imply an appropriate value of ϵ_{MEC} in medium-heavy nuclei. Accurate values of the weak couplings are needed in order to produce accurate spectra to be used in the reactor-antineutrino analyses as well as analyses of the backgrounds in rare-event searches.

References

[1] K. Kubodera, J. Delorme, M. Rho, Phys. Rev. Lett. 40 (1978) 755.
[2] P. Guichon, M. Giffon, J. Joseph, R. Laverriere, C. Samour, Z. Phys. A 285 (1978) 183.

[3] P. Guichon, M. Giffon, C. Samour, Phys. Lett. B 74 (1978) 15.
[4] I.S. Towner, F.C. Khanna, Nucl. Phys. A 372 (1981) 331.
[5] J. Delorme, Nucl. Phys. A 374 (1982) 541c.
[6] E.K. Warburton, I.S. Towner, B.A. Brown, Phys. Rev. C 49 (1994) 824.
[7] E.K. Warburton, J.A. Becker, B.A. Brown, D.J. Millener, Ann. Phys. 187 (1988) 471.
[8] E.K. Warburton, Phys. Rev. C 44 (1991) 233.
[9] K. Kubodera, M. Rho, Phys. Rev. Lett. 67 (1991) 3479.
[10] M. Haaranen, P.C. Srivastava, J. Suhonen, Phys. Rev. C 93 (2017) 034308.
[11] J. Kostensalo, M. Haaranen, J. Suhonen, Phys. Rev. C 95 (2017) 044313.
[12] J. Kostensalo, J. Suhonen, Phys. Rev. C 96 (2017) 024317.
[13] M. Haaranen, J. Kotila, J. Suhonen, Phys. Rev. C 95 (2017) 024327.
[14] J.C. Hardy, I.S. Towner, V. Koslowsky, E. Hagberg, H. Schmeig, Nucl. Phys. A 509 (1990) 429.
[15] H. Behrens, W. Bühring, Electron Radial Wave Functions and Nuclear Beta-decay, Clarendon Press, Oxford, 1982.
[16] B.A. Brown, W.D.M. Rae, Nucl. Data Sheets 120 (2014) 115.
[17] H. Mach, E.K. Warburton, R.L. Gill, R.F. Casten, J.A. Becker, B.A. Brown, J.A. Wigner, Phys. Rev. C 41 (1991) 226.
[18] D.H. Gloeckner, Nucl. Phys. A 253 (1975) 301.
[19] X. Ji, B.H. Wildenthal, Phys. Rev. C 37 (1988) 1256.
[20] B.A. Brown, unpublished.
[21] B.A. Brown, N.J. Stone, J.R. Stone, I.S. Towner, M. Hjorth-Jensen, Phys. Rev. C 71 (2005) 044317.
[22] E.K. Warburton, B.A. Brown, Phys. Rev. C 43 (1991) 602.
[23] C.M. Baglin, Nucl. Data Sheets 113 (2012) 2187.
[24] C.M. Baglin, Nucl. Data Sheets 112 (2011) 1163.
[25] S.K. Basu, G. Mukherjee, A.A. Sonzogni, Nucl. Data Sheets 111 (2010) 2555.
[26] D. Abriola, A.A. Sonzogni, Nucl. Data Sheets 109 (2008) 2501.
[27] N. Nica, Nucl. Data Sheets 111 (2010) 525.
[28] Y. Khazov, A. Rodionov, F.G. Kondev, Nucl. Data Sheets 112 (2011) 855.
[29] A.A. Sonzogni, Nucl. Data Sheets 103 (2004) 1.
[30] B. Singh, A.A. Rodionov, Y.L. Khazov, Nucl. Data Sheets 109 (2008) 517.
[31] E. Browne, J.K. Tuli, Nucl. Data Sheets 108 (2007) 2173.
[32] J. Chen, Nucl. Data Sheets 146 (2017) 1.
[33] P.K. Joshi, B. Singh, S. Singh, Nucl. Data Sheets 138 (2016) 1.
[34] T.D. Johnson, D. Symochko, M. Fadil, J.K. Tuli, Nucl. Data Sheets 112 (2011) 1949.
[35] E. Browne, J.K. Tuli, Nucl. Data Sheets 113 (2012) 715.
[36] E.A. Mccutchan, C.M. Baglin, O. Gorbachenko, N. Todorovic, Nucl. Data Sheets 114 (2013) 661.
[37] M.S. Basunia, Nucl. Data Sheets 108 (2007) 633.
[38] M. Kirchbach, H. Reinhardt, Phys. Lett. B 208 (1988) 79.
[39] W.T. Chou, E.K. Warburton, B.A. Brown, Phys. Rev. C 47 (1993) 163.
[40] B.H. Wildenthal, M.S. Curtin, B.A. Brown, Phys. Rev. C 28 (1983) 1343.
[41] T. Siiskonen, M. Hjorth-Jensen, J. Suhonen, Phys. Rev. C 63 (2001) 055501.
[42] C. Buck, A.P. Collin, J. Haser, M. Lindner, Phys. Lett. B 765 (2017) 159.